UvA-DARE (Digital Academic Repository)

UV and X-ray observations of the neutron star LMXB EXO 0748-676 in its quiescent state

Parikh, A.S.; Degenaar, N.; Hernández Santisteban, J.V.; Wijnands, R.; Psaradaki, I.; Costantini, E.; Modiano, D.; Miller, J.M.

[Link to publication](#)

UV and X-ray observations of the neutron star LMXB EXO 0748–676 in its quiescent state

A. S. Parikh,[1] N. Degenaar [iD],[1]★ J. V. Hernández Santisteban,[1,2] R. Wijnands,[1] I. Psaradaki,[1,3] E. Costantini,[1,3] D. Modiano[1] and J. M. Miller[4]

[1]*Anton Pannekoek Institute for Astronomy, University of Amsterdam, Science Park 904, NL-1098 XH Amsterdam, the Netherlands*
[2]*School of Physics and Astronomy, University of St. Andrews, North Haugh, St. Andrews, Fife KY16 933, UK*
[3]*SRON Netherlands Institute for Space Research, Sorbonnelaan 2, NL-3584 CA Utrecht, the Netherlands*
[4]*Department of Astronomy, University of Michigan, 1085 South University Avenue, Ann Arbor, MI 48109, USA*

ABSTRACT

The accretion behaviour in low-mass X-ray binaries (LMXBs) at low luminosities, especially at $<10^{34}\,\mathrm{erg\,s^{-1}}$, is not well known. This is an important regime to study to obtain a complete understanding of the accretion process in LMXBs, and to determine if systems that host neutron stars with accretion-heated crusts can be used probe the physics of dense matter (which requires their quiescent thermal emission to be uncontaminated by residual accretion). Here, we examine ultraviolet (UV) and X-ray data obtained when EXO 0748–676, a crust-cooling source, was in quiescence. Our *Hubble Space Telescope* spectroscopy observations do not detect the far-UV continuum emission, but do reveal one strong emission line, C IV. The line is relatively broad ($\gtrsim$3500 km s^{-1}), which could indicate that it results from an outflow such as a pulsar wind. By studying several epochs of X-ray and near-UV data obtained with *XMM–Newton*, we find no clear indication that the emission in the two wavebands is connected. Moreover, the luminosity ratio of $L_\mathrm{X}/L_\mathrm{UV} \gtrsim 100$ is much higher than that observed from neutron star LMXBs that exhibit low-level accretion in quiescence. Taken together, this suggests that the UV and X-ray emission of EXO 0748–676 may have different origins, and that thermal emission from crust-cooling of the neutron star, rather than ongoing low-level accretion, may be dominating the observed quiescent X-ray flux evolution of this LMXB.

Key words: accretion, accretion discs – ultraviolet: general – X-rays: binaries.

1 INTRODUCTION

Low-mass X-ray binaries (LMXBs) are systems wherein a compact object accretes matter from a companion star via an accretion disc. Many LMXBs exhibit transient behaviour and for these sources the accretion of matter on to the compact object is expected to (almost) stop during quiescence (e.g. Lasota 2001; Hameury 2020). The outburst luminosities exhibited by transient LMXBs hosting neutron stars (NSs) are typically of the order of 10^{35}–10^{38} erg s^{-1} in the 0.5–10 keV energy range (e.g. Yan & Yu 2015). In transient systems, these luminosities drop to levels of 10^{30}–10^{34} erg s^{-1} when the outbursts cease (see e.g. Wijnands, Degenaar & Page 2017, for a review).

During the brightest phases of an outburst, typically at luminosities $\gtrsim 10^{36}$ erg s^{-1}, the accretion flow takes on the form of a geometrically thin, optically thick disc (e.g. Shakura & Sunyaev 1973; Lasota 2001). The disc may be accompanied by a corona, a Comptonising medium of hot electrons, likely located close to the central compact object (e.g. Done, Gierliński & Kubota 2007; Gilfanov 2010). The properties of the accretion flow close to the compact object are thought to change significantly towards lower luminosities by (eventually) transitioning into a geometrically thick, optically thin flow also referred to as a radiatively inefficient accretion flow (RIAF; e.g. Narayan & Yi 1994; Dubus, Hameury & Lasota 2001). However,

the conditions at which the transition from a standard disc to an RIAF take place are not very well understood, and hardly constrained by observations.

Studies of quiescent accretion flows are further exacerbated, as the inherent low luminosities exhibited in this state make it difficult to obtain high-quality data. The mere presence and properties of a disc, corona and/or RIAF at these luminosities is not definitively known (e.g. Hynes & Haswell 1999; Hynes, Robinson & Bitner 2005; Cackett et al. 2013a), so it is not clear if, and how, accretion takes place. Accretion on to the compact object could potentially come to a halt in quiescence, but there could also be ongoing inward motion of the material through a disc/corona/RIAF, perhaps still enabling low-level accretion on to the compact object. Studies in quiescence are important to understand accretion at low luminosities and contribute to our overall understanding of accretion processes in LMXBs.

Apart from studying accretion, transient NS LMXB systems can also be used as laboratories to probe the properties of dense matter present in NS crusts and cores (e.g. Brown, Bildsten & Rutledge 1998; Cumming et al. 2017; Wijnands et al. 2017). During outbursts, the accreted matter compresses the NS crust and induces reactions such as electron captures, neutron emissions, and density-driven fusion reactions (e.g. Haensel & Zdunik 1990, 2008; Steiner 2012). These reactions release heat in the crust, disrupting its thermal equilibrium with the core. Furthermore, observations of NS LMXBs have indicated that, in addition to these theoretically predicted heating reactions, energy may also be released at shallow depths

★ E-mail: degenaar@uva.nl

in the crust by an unknown 'shallow heating' process (e.g. Brown & Cumming 2009; Degenaar, Brown & Wijnands 2011b; Degenaar et al. 2014).

With the cessation of an outburst, i.e. active accretion, the compression-induced heating reactions occurring in the NS crust are expected to stop. As a result, in quiescence the crust cools to reinstate the thermal equilibrium with the core. Monitoring this cooling evolution and comparing it to theoretical models has been used to investigate the behaviour of the dense matter present in NS crusts (e.g. Rutledge et al. 2001; Wijnands et al. 2001; Shternin et al. 2007; Brown & Cumming 2009; Page & Reddy 2013; Turlione, Aguilera & Pons 2015; Ootes et al. 2018). So far, such crust-cooling studies have been carried out for 10 NSs in LMXBs by examining their X-ray spectral evolution (see Wijnands et al. 2017, for a review). The quiescent spectra of NSs exhibiting crust cooling are typically characterized by a prominent thermal emission component (often contributing >70 per cent of the total 0.5–10 keV flux) that is interpreted as heat radiation from the NS surface.

For several NSs in LMXBs there is evidence that some form of low-level accretion is occurring, either continuously or in spurts, at similarly low luminosities as are exhibited by crust-cooling sources in quiescence (e.g. EXO 1745–248, Cen X-4, Aql X-1, XTE J1701–462; Fridriksson et al. 2011; Degenaar & Wijnands 2012; Bernardini et al. 2013; Coti Zelati et al. 2014). Notably, the spectra of these sources are characterized by a prominent power-law shaped emission component that, when detailed studies are possible, appears to extend to energies >10 keV (Chakrabarty et al. 2014). Often this power-law emission component occurs alongside a thermal emission component. Indeed, theoretical calculations suggest that low-level accretion on to a NS can produce a composite spectrum of thermal and power-law-like emission components (e.g. Deufel, Dullemond & Spruit 2001).

Several crust-cooling sources also require a power-law shaped component, in addition to thermal surface emission, to adequately fit their quiescent spectra (e.g. Degenaar et al. 2009; Wijnands et al. 2015; Parikh et al. 2017). This could potentially indicate that low-level accretion is ongoing in these systems. If true, it is not trivial to disentangle contributions of low-level accretion and crust-cooling emission to the thermal emission spectra. This then complicates our determination of the crust-cooling evolution and thereby the inferred NS physics. Constraining the properties of low-level accretion in LMXBs is therefore also important to correctly infer the physics of the NS crust and core.

In addition to examining the X-ray spectra, accretion can also be probed at ultraviolet (UV) wavelengths. The surface temperatures of NSs in LMXBs are generally such ($\simeq 10^6 - 10^7$ K) that their cooling emission is not expected to significantly contribute to their UV emission. Also, the inherent emission from the late-type companion star contributes negligibly to the UV emission of the system. However, the accretion stream, arising from the Roche lobe overflow of the donor star, is expected to be UV bright, hence making the UV a suitable wavelength regime to probe the quiescent accretion flows. Previous studies of quiescent LMXBs have indicated that the UV emission arises from small emitting radii with unexpected high temperatures, suggesting that this does not come from the bulk of the disc but rather from the impact point of matter from the companion star hitting the accretion disc (e.g. Froning et al. 2011), or X-ray irradiation of the inner accretion disc or companion star (e.g. Hynes & Robinson 2012; Bernardini et al. 2013; Cackett et al. 2013a).

A further indicator of possible ongoing accretion towards the NS can be derived from the correlation exhibited between the X-ray and UV luminosities in quiescence (e.g. Hynes & Robinson 2012). In particular, if the UV and X-ray luminosities are similarly bright, the UV emission is too high to only arise from irradiation of the disc (if present) and/or the companion star by X-rays from the central compact object (or from a hot inner accretion disc, if present).

Most NS LMXBs cannot be studied in the UV as they exhibit strong interstellar extinction along the line of sight. However, a few LMXBs exhibit less strong extinction, allowing us to probe for signatures of low-level accretion in the UV. One such source is the crust-cooling source EXO 0748–676.

1.1 The NS LMXB EXO 0748–676

The NS LMXB EXO 0748–676 (UY Vol) was discovered almost three decades ago (Parmar et al. 1985). It exhibited X-ray eclipses (lasting $\simeq 500$ s), indicating that the binary is viewed at high inclination ($i \simeq 75°-83°$). Its orbital period was determined to be $\simeq 3.8$ h (Parmar et al. 1986; Wolff et al. 2009). The source displayed thermonuclear X-ray bursts, which indicated the NS nature of the primary and resulted in a distance estimate of $\simeq 7.4$ kpc (Wolff et al. 2005).

EXO 0748–676 exhibited an accretion outburst that is estimated to have started between 1980 and 1984 (Degenaar et al. 2009). It remained active until 2008 September (Hynes & Jones 2008; Torres et al. 2008; Wolff, Ray & Wood 2008a; Wolff et al. 2008b). Observations of the source in quiescence indicate that the crust of the NS was heated during outburst and exhibited cooling in quiescence (e.g. Degenaar et al. 2009, 2011a, 2014; Díaz Trigo et al. 2011; Cheng et al. 2017). However, more recent quiescent observations, obtained >2000 d after the end of its accretion outburst, indicate a rise in the observed effective NS temperature (Parikh et al. 2020). This rise is highly surprising for a crust-cooling source as it is expected to exhibit a continuous decay in the temperature rather than a rise. In this work, we investigate if low-level accretion occurs in the quiescent state of EXO 0748–676.

2 OBSERVATIONS AND DATA ANALYSIS

We examine UV spectroscopic and imaging data of EXO 0748–676. We also compare these UV data with (quasi-)simultaneous X-ray data. De-reddened photometric fluxes and magnitudes were calculated by assuming $E(B - V) = 0.06$ (Hynes et al. 2006) and the Galactic extinction curves of Cardelli, Clayton & Mathis (1989). The de-reddening has been carried out in PYTHON using the EXTINCTION package.[1] All uncertainties reflect 1σ confidence levels.

2.1 *Hubble Space Telescope* observations

2.1.1 Far-UV spectroscopy

We obtained far-UV (FUV) spectroscopic observations of EXO 0748–676 in quiescence using the Cosmic Origins Spectrograph (COS; Green et al. 2012) on board the *Hubble Space Telescope* (*HST*) under the GO programme 13108 (PI: Degenaar). The source was targeted for nine orbits divided over two visits, starting on 2013 March 28 (MJD 56379). The total on-source exposure time amounted to $\simeq 7.4$ h. The COS was operated using the low-resolution G140L grating with segment B switched off. This provided FUV coverage in the wavelength range of $\simeq 1118-2251$ Å with a resolving power of $\lambda/\Delta\lambda \simeq 2500-3500$ Å. For each exposure, the grating was stepped through different fp-pos positions to minimize the fixed pattern noise.

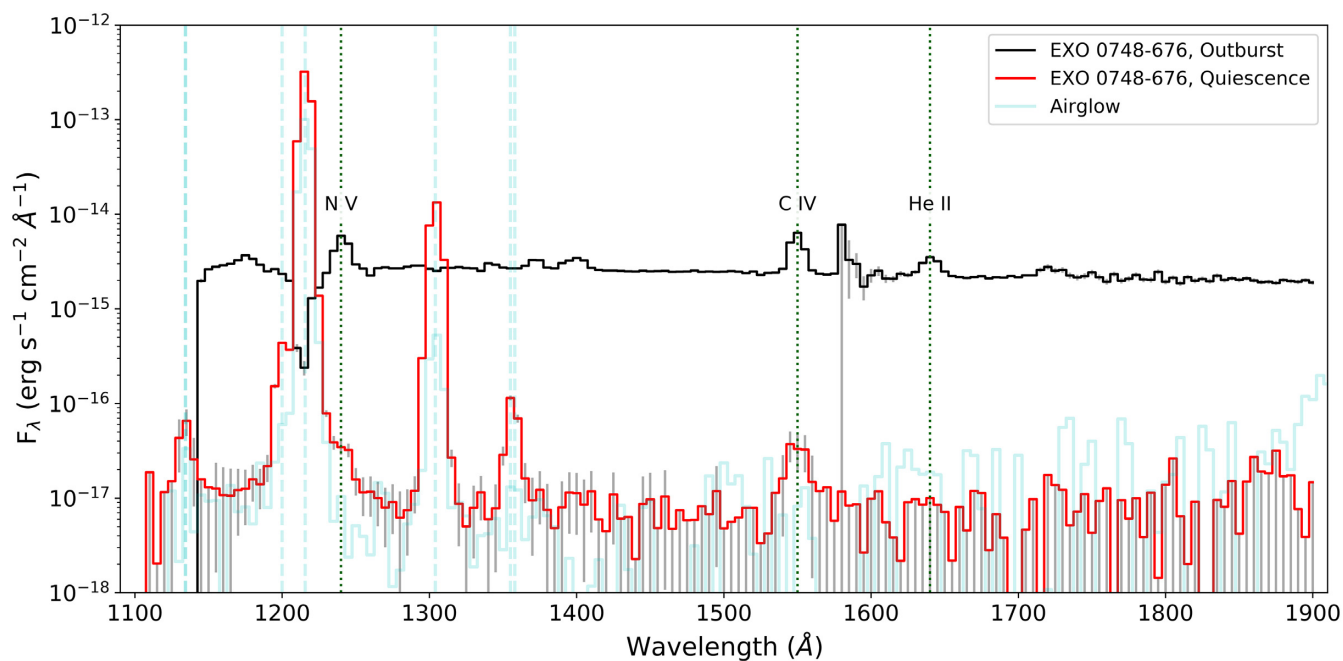[1] https://extinction.readthedocs.io/en/latest/

Figure 1. Co-added FUV spectra of EXO 0748–676 obtained using *HST* during two epochs – during outburst (using STIS, black) and during quiescence (using COS, red). The respective error bars are shown in grey. Both spectra have been re-binned to the same spectral resolution (of $\Delta\lambda = 5$ Å). The vertical, dotted, green lines indicate the strong emission lines seen in the outburst spectra, as identified by Pearson et al. (2006). The spectrum shown in blue is an example of the airglow spectrum as observed using the COS instrument. The vertical, dashed, blue lines are often-observed airglow emission lines exhibited during observations obtained using COS (e.g. Froning et al. 2014). The STIS observation does not suffer from contamination due to airglow.

All the data were taken in TIME-TAG mode. These COS data were retrieved from the Multi-Mission Archive at STScI.[2] The downloaded data had been pre-processed with CALCOS (version 3.3.7).

To contextualize the quiescent FUV spectra of EXO 0748–676, we compared it to the FUV spectrum obtained during outburst. This outburst spectrum was obtained in 2003 February 18 (MJD 52688) using the Space Telescope Imaging Spectrograph (STIS; e.g. Ely et al. 2015). The source was observed for $\simeq$9 h over two complete orbits in the continuous viewing zone. The observations were carried out using the FUV MAMA detector (Joseph et al. 1995) and the G140L grating. The data were taken in the TIME-TAG mode. The STIS data were retrieved from the Multi-Mission Archive at STScI and were pre-processed with CALSTIS (version 3.4.2). Further details of these data are provided in Hynes et al. (2006) and Pearson et al. (2006).

Spectral analysis on these FUV data was performed on the products downloaded from the archive. The various one-dimensional spectra, corresponding to each quiescent epoch, were combined using the SPLICE task in IRAF[3] (e.g. Tody 1986). These spectra were further analysed using the SPECUTILS package[4] (Astropy-Specutils Development Team 2019) in PYTHON and are shown in Fig. 1. Line widths were calculated based on Gaussian fits using LINE_FLUX, part of the SPECUTILS package in PYTHON.

2.1.2 Near-UV photometry

Each of the two *HST* visits of EXO 0748–676 during quiescence were preceded by acquisition imaging observations of 51 s each,

using mirror A and the PSA aperture. This provided sensitivity in the UV range of $\simeq$1600–3300 Å, peaking at $\simeq$2300 Å.

We estimated a near-UV (NUV)[5] magnitude for EXO 0748–676 from these acquisition images. Source events were extracted from an aperture of radius 0.10 arcsec using PYTHON. Furthermore, an aperture of three times that size was used to estimate the background. The detected count rates were converted to fluxes using the count rate to flux conversion factor appropriate for our instrumental set-up. This conversion factor, reported in the headers of the acquisition images, was found to be 1 counts s^{-1} = 4.82×10^{-18} erg cm^{-2} s^{-1} Å^{-1}.

2.2 *Swift* observations

EXO 0748–676 was observed with the X-ray telescope (XRT; Burrows et al. 2005) on board the *Neil Gehrels Swift Observatory* (*Swift*; Gehrels et al. 2004). A $\simeq$7.8 ks observation was carried out on 2013 March 23 (MJD 56374), i.e. 5 d before the *HST* UV observations were obtained. We reduced the *Swift* data[6] using the HEASOFT package (version 6.13), by re-processing the data using the XRTPIPELINE. We extracted the spectrum of the source with XSELECT using a circular region with a radius of 35 arcsec centred on EXO 0748–676. A surrounding annular region, having an inner and outer radius of 100 and 200 arcsec, respectively, was used to obtain a background spectrum. The spectral data were grouped into bins with a minimum of 10 photons per bin using the HEASOFT tool GRPPHA. The spectrum was fit using XSPEC.

---

[2] https://archive.stsci.edu/hst/search.php
[3] https://iraf-community.github.io/install.html
[4] https://specutils.readthedocs.io/en/stable/index.html

[5] In this paper, we define NUV to encompass all data in the wavelength range 1600–3000 Å. These include the NUV data discussed in Sections 2.1.2, 2.2, and 2.3.
[6] Obtained from the *Swift* archive, found at https://heasarc.gsfc.nasa.gov/cgi-bin/W3Browse/swift.pl

Table 1. Log of the (quasi-)simultaneous UV and X-ray observations of EXO 0748–676 in quiescence.

Epoch	MJD	Observatory	UV band	Central UV wavelength[a] (Å)	UV λL_λ ($\times 10^{31}$ erg s^{-1})	Unabsorbed L_X ($\times 10^{32}$ erg s^{-1})	L_X/L_{UV} ratio
1	54776.4	*XMM–Newton*	*UVW1*	2910	<47.8	64.7 ± 0.5	>13.5
2	54908.0	*XMM–Newton*	*U*	3400	8.4 ± 2.4	49.6 ± 0.3	≃59.1
3	55364.2	*XMM–Newton*	*U*	3400	<3.8	43.9 ± 0.3	>115.5
4	55376.5[b]	*HST* and *Swift*	NUV	2300	≃1.8	34.7 ± 2.6	≃243.9
5	56397.2	*XMM–Newton*	*U*	3400	<4.0	35.9 ± 0.2	>89.8
6	58240.3	*XMM–Newton*	*U*	3400	4.9 ± 1.4	40.9 ± 0.2	≃83.5

Notes. We have assumed $D = 7.4$ kpc and $E(B - V) = 0.06$. We caution that the UV luminosities quoted here assume a flat spectral shape; see Section 3.2.4 for a discussion on the impact of the unknown spectral shape.
[a]Obtained from https://www.swift.ac.uk/analysis/uvot/filters.php.
[b]The MJD for this epoch has been determined by averaging the MJD of the *HST* and *Swift* observations

Since EXO 0748–676 hosts a cooling NS crust (e.g. Parikh et al. 2020, see the references therein for more details), we fitted the XRT spectrum with NSATMOS (a NS atmosphere model; Heinke et al. 2006). The source distance was set to $D = 7.4$ kpc (e.g. Galloway, Özel & Psaltis 2008) and the NS mass and radius to $M = 1.6\,M_\odot$ and $R = 12$ km, respectively. Given the limited statistics of the XRT data, we fixed several of the NSATMOS parameters to the values obtained from fitting high-quality quiescent *Chandra* and *XMM–Newton* spectra of EXO 0748–676 (see Parikh et al. 2020, for details, where the same parameters were fixed). An additional power-law component was needed to fit some high-quality quiescent spectra of this source (Parikh et al. 2020). Thus, we also use this component for the XRT spectral fitting here. The power-law index was fixed to $\Gamma = 1.0$ and the normalization was free to vary. In addition, we fix the column density to $N_H = 4.3 \times 10^{20}$ cm^{-2}, as determined from fitting high-quality data, presented in Parikh et al. (2020).

Alongside the XRT, *Swift* hosts the UltraViolet Optical Telescope (UVOT; Roming et al. 2005), with NUV photometric and spectroscopic capabilities. We examined all archival UVOT data. We processed the data using the UVOUSOURCE tool. However, the source was not detected by the UVOT during any quiescent observations. Since the upper limits obtained from these data were not constraining, we do not discuss them further.

2.3 *XMM–Newton* observations

The *X-ray Multi-Mirror Mission* or *XMM–Newton* hosts instruments with observation capabilities in the X-ray and NUV wavelength regimes. This allows for correlated X-ray–UV studies as instruments observing in both wavelength ranges operate simultaneously. So far, EXO 0748–676 has been observed six times during quiescence using *XMM–Newton*. These observations were downloaded from the *XMM–Newton* archive.[7]

The X-ray data, obtained using the European Photon Imaging Camera (EPIC; Strüder et al. 2001; Turner et al. 2001), were processed by extracting the spectra and fitting them collectively in XSPEC. The details of the spectral extraction and spectral fitting are provided in section 2 of Parikh et al. (2020).

The NUV photometric data, obtained using the Optical Monitor (OM; Mason et al. 2001), were only available for five of the six observations. This is because the data for observation 3 (corresponding to observation Id 0605560501) were not obtained due to a technical error (Díaz Trigo et al. 2011). For the available data, the NUV fluxes were extracted using the OM tasks OMICHAIN and OMFCHAIN in

SAS, as was appropriate when the photometric data were obtained in the imaging mode and in the fast mode, respectively. We examined the fluxes corresponding to the full exposure (for each available filter, from the output files produced by OMICHAIN and OMFCHAIN) from each entire observation, in order to use the most constraining flux estimate for a given epoch. Furthermore, this is because we do not expect to be able to detect any orbital variations in the flux due to the low UV luminosities exhibited by EXO 0748–676 (as was shown by Díaz Trigo et al. 2011, during the earliest quiescent UV observations obtained). EXO 0748–676 was not detected during several OM observations (see Table 1). In case of non-detections, we used the faintest detected source in the associated observation as an upper limit estimate for EXO 0748–676 (see Table 1). This was done by examining the output files produced by OMICHAIN and OMFCHAIN. Since the default detection threshold is 3σ, our obtained upper limits correspond to this significance level.

3 RESULTS

3.1 The *HST* FUV spectra

3.1.1 Quiescent spectrum

Despite the low extinction towards EXO 0748–676, the quality of the quiescent FUV spectra obtained by *HST* during individual orbits was low. This was due to the inherently low source flux in quiescence. The signal-to-noise ratio was inadequate to perform any phase-resolved spectral analysis that is necessary to investigate signatures of the orbital motion. We, therefore, combined individual exposures into a uniform wavelength grid (with $\Delta\lambda = 5$ Å) and applied an error-weighted average using the SPECTRES package (Carnall 2017) in PYTHON. The resulting averaged spectrum is shown in red in Fig. 1. Although we combined the different COS exposures, the resulting spectrum was still of low signal-to-noise ratio and there was no continuum emission detected above $\simeq 10^{-17}$ erg cm^{-2} s^{-1} Å^{-1}, preventing us from obtaining any continuum flux measurement from the FUV spectral data.

3.1.2 Outburst spectrum

We aim to qualitatively compare the outburst spectrum to that obtained during quiescence and are not interested in probing the orbital variations observed during the outburst. Thus, the individual STIS spectra were combined into one spectrum and as a result, this blurs out the orbital variations observed in outburst (Pearson et al. 2006). This was done as described in Section 2.1.1. To ensure direct comparison with the quiescent spectrum, the combined

outburst spectrum was re-binned to the same resolution (of $\Delta\lambda = 5$ Å) as that of the combined quiescent spectrum. This is shown in Fig. 1, in black. The dotted, green, vertical lines indicate the significant emission lines in the outburst spectrum, as identified by Pearson et al. (2006). The emission observed near 1580 Å is an artefact and does not correspond to any line (Pearson et al. 2006).

3.1.3 Airglow observed by the COS instrument

Airglow is the contribution of emission from the Earth's atmosphere. The quiescent FUV spectrum is shown alongside an example of a spectrum obtained using the same COS instrument when the terrestrial airglow was strongly observed.[8] This is shown in blue in Fig. 1 and has been re-binned to have the same spectral resolution as the quiescent source spectrum. As can be seen, this airglow spectrum roughly matches the strong emission lines seen around 1200, 1215, and 1304 Å in our quiescent spectrum of EXO 0748–676. Evidence from other airglow observations, obtained using COS, show that the emission line observed around 1356 Å is also a result of airglow (e.g. Froning et al. 2014). The prominent wavelengths at which airglow emission lines are expected is shown using vertical, dashed, blue lines. The outburst spectra were taken with a different instrument and do not suffer from airglow (Pearson et al. 2006).

Discarding any emission lines due to airglow, we find that our quiescent observation of EXO 0748–676 only exhibits one significant emission line around 1550 Å, identified to be the C IV line by Pearson et al. (2006). Due to the lack of a continuum detection, only the lower limit of the C IV line could be constrained during quiescence. This C IV emission line has a width of $\simeq 19.5$ and $\gtrsim 18.2$ Å in the spectrum obtained during outburst and quiescence, respectively.

We also investigated if any other lines that were significant during the outburst were present in quiescence. The red wing of the emission line in the quiescent spectra, observed around 1220 Å, exhibits an excess as compared to the corresponding airglow emission line. This may be indicative of a N V emission line from the source, as was seen during outburst (see Fig. 1; see also Pearson et al. 2006). This excess is relative to our choice of the example airglow emission spectrum shown. However, it is not trivial to constrain any excess in the spectrum due to emission by the N V line in quiescence.

3.2 The ratio of the X-ray and UV luminosities

We examined quasi-simultaneous epochs of X-ray and NUV data to investigate the correlation between emission in these two energy bands.

3.2.1 HST *NUV photometry*

Visual inspection of the NUV acquisition images obtained by the *HST*/COS show that EXO 0748–676 was faintly detectable. Examining these images, we estimated an average (background-subtracted) source count rate of $\simeq 0.16$ counts s^{-1}. Using the appropriate count rate to flux conversion factor (see Section 2.1.2), we estimated a flux density of $F_\lambda \simeq 7.3 \times 10^{-19}$ erg cm^{-2} s^{-1} Å^{-1}, and an AB magnitude of $\simeq 26.1$ mag. The de-reddened flux density

and magnitude were found to be $F_\lambda \simeq 1.2 \times 10^{-18}$ erg cm^{-2} s^{-1} Å^{-1} and $\simeq 25.6$ mag, respectively.

By multiplying the flux with the central wavelength of the instrument passband (2300 Å; Holland et al. 2012), we estimate a de-reddened UV flux of $F_{\mathrm{UV}} \simeq 2.8 \times 10^{-15}$ erg cm^{-2} s^{-1}. For a distance of 7.4 kpc, this translates into a luminosity of $L_{\mathrm{UV}} \simeq 1.8 \times 10^{31}$ erg s^{-1}. We note, however, that this approach effectively assumes that the UV spectrum is flat over the instrument passband, which is not necessarily the case. We investigate the effect of this assumption in Section 3.2.4.

3.2.2 Swift *X-ray data*

The model described in Section 2.2 provided a good description of the X-ray spectral data ($\chi_\nu^2 = 0.97$ for 31 degrees of freedom). We obtained $kT_{\mathrm{eff}}^\infty = 111.3 \pm 2.0$ eV and the resulting unabsorbed flux was $F_X = (5.3 \pm 0.4) \times 10^{-13}$ erg cm^{-2} s^{-1}, in the 0.5–10 keV energy range. At a distance of 7.4 kpc, this corresponds to a luminosity of $L_X = (3.5 \pm 0.3) \times 10^{33}$ erg s^{-1}. Thus, using our quiescent quasi-simultaneous *Swift* X-ray and *HST* NUV observations, we obtain a luminosity ratio of $L_X/L_{\mathrm{UV}} \simeq 200$.

3.2.3 XMM–Newton *X-ray and UV data*

EXO 0748–676 was detected two times in quiescence using the OM with the *U* filter (see Table 1). Upper limits were obtained during three other epochs – once using the *UVW1* filter and twice using the *U* filter. The results of the OM photometry is listed in Table 1. The source was detected in X-ray during all the *XMM–Newton* epochs reported here (i.e. those with accompanying OM observations, see Section 2.3). Details about the X-ray luminosities are presented in Parikh et al. (2020, see their table 1).

If we calculate the UV luminosity by multiplying the inferred UV fluxes with the filter width (but see Section 3.2.4), we obtain L_X/L_{UV} ratios of $\simeq 100$ from the *XMM–Newton* data (see Table 1). This is of the same order of magnitude as the ratio inferred for the epoch of quasi-simultaneous *HST* and *Swift* observations (see Section 3.2.2).

3.2.4 *The effect of the unknown UV spectral shape*

In Sections 3.2.1 and 3.2.3, we estimated λL_λ for all UV observations in order to compare the X-ray and UV luminosity ratio of EXO 0748–676 with that of the eight LMXBs studied in Hynes & Robinson (2012). However, the UV spectrum is likely not flat and may significantly change across the wavelength range that we study. To probe the magnitude of this effect, we folded a blackbody through the relevant UV filter to determine the expected ratio of fluxes in different wavebands for each observation.[9] For this exercise, we used two different temperatures, of 5000 and 13 000 K, based on the UV-optical spectral energy distributions (SEDs) of the eight quiescent LMXBs studied in Hynes & Robinson (2012). We scaled the two different SEDs by performing synthetic photometry on them and comparing them to the unabsorbed fluxes from Table 1. We then integrated the fluxes and compared these to a flat spectrum (i.e. the implicit assumption when calculating λL_λ).

We show the results of these calculations for each observation in Fig. A1. The SED shape has the largest effect on the UV luminosity

---

[8]The different observations of airglow by the *HST*/COS can be found at https://www.stsci.edu/hst/instrumentation/cos/calibration/airglow. We show the airglow spectrum corresponding to the dataset LBW3E4060, observed on 2012 August 10 (MJD 56149).

[9]The response for the *HST*/COS acquisition image is not available, so we took the WFC3/UVIS *F218W* filter for this as a proxy.
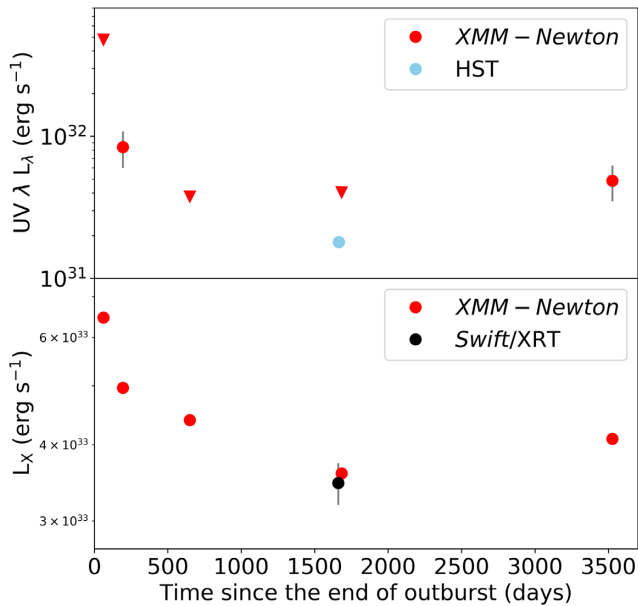
Figure 2. The top and bottom panels show the quasi-simultaneous evolution of the UV and X-ray luminosity of EXO 0748–676 during quiescence. The data from the quasi-simultaneous *HST* and *Swift* observations are shown in blue and black, respectively. The red data indicate those observations obtained using *XMM–Newton*. All upper limits are marked by downward-facing triangles. We note that the plotted UV data do not take into account uncertainties on the UV spectral shape, which most strongly affect the bluest filters; caution should therefore be taken in comparing the luminosities for the first *XMM–Newton* (*UVW1* filter) and the *HST* data points to the other *XMM–Newton* (*U* filter) data points (see Section A1).

calculation for the bluest filters. For instance, for the OM/*UVW1* filter the ratio of the integrated flux from the reddest SED (i.e. the one with a blackbody temperature of 5000 K) compared to a flat spectrum is a factor $\simeq 1.3$, and for the *HST* acquisition image this ratio is estimated to be a factor $\simeq 2.6$. The magnitude of the effect in the *U* band is much smaller, of the order of 10 per cent (see Fig. A1).

3.2.5 L_X versus L_{UV}

The unabsorbed X-ray luminosities in the 0.5–10 keV energy range, along with the (quasi-)simultaneously obtained UV luminosities (corrected for extinction) are summarized in Table 1 and shown in Figs 2 and 3. In the X-rays, EXO 0748–676 shows a steady decrease by about 40 per cent over the $\simeq 9.5$ yr time span covering the observations (see also Parikh et al. 2020). In the UV band, such long-term variations are not clearly seen.

EXO 0748–676 was not detected in the UV during the first *XMM–Newton* epoch, when the OM was used with the *UVW1* filter. However, the obtained upper limit is not constraining and much higher than the *U*-band luminosities measured at later times. During the second and last *XMM–Newton* epochs, EXO 0748–676 is detected in the *U* filter at luminosities of $\simeq 8.5$ and 5×10^{31} erg s^{-1}, respectively, but with large errors; the two data points are consistent within 2σ even without taking into account the additional $\simeq 10$ per cent uncertainty of the UV spectral shape in this band (see Section 3.2.4). The X-ray luminosity corresponding to these two data points differs by about 20 per cent. EXO 0748–676 is not detected in the *U*-band in the other two observations, but the obtained upper limits are not significantly smaller than the *U*-band luminosities inferred for the two detections.
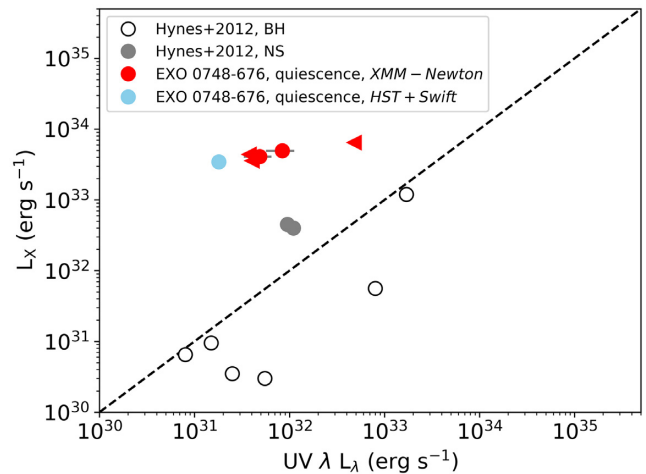

Figure 3. The observed X-ray versus UV luminosity of EXO 0748–676 during six quiescent epochs is shown. Five epochs were obtained using *XMM–Newton* (shown in red). One epoch was observed using *HST* and the *Swift*, and is shown in blue. We note that these data points do not take into account the unknown UV spectral shape (see Section A1). We compare EXO 0748–676 to eight other quiescent LMXBs studied in Hynes & Robinson (2012). The six systems hosting BHs are shown by open black circles and represent GRO J0422+32 (V518 Per), MM Vel, XTE J118–40, A0620–00, GU Mus, and V404 Cyg (listed in ascending order of the UV luminosity). The two NS systems are shown by filled grey circles and correspond to Aql X-1 and Cen X-4. All upper limits are marked by triangles facing the relevant direction.

While the inferred luminosity from the *HST* acquisition image is a factor of a few lower than the *U*-band luminosities measured with *XMM–Newton* (see Table 1 and Fig. 2), the unknown UV spectral shape introduces large errors in this band (see Section 3.2.4). The available data thus do not indicate that there are strong variations in the UV emission of EXO 0748–676 over the $\simeq 9.5$-yr observing period. However, the uncertainties are large and variations of similar magnitude as seen in the X-rays ($\simeq 40$ per cent) cannot be excluded.

Fig. 3 also shows the X-ray versus UV luminosity for other NS and BH LMXBs observed in quiescence, as reported by Hynes & Robinson (2012). It is clear from this plot that while the UV luminosity of EXO 0748–676 is in the same realm as that observed for other LMXBs, its X-ray luminosity, and hence its X-ray/UV luminosity ratio, is much larger than that of any of the other systems.

4 DISCUSSION

Investigating quiescent spectra of LMXBs allow us to understand the accretion behaviour in these systems at low luminosities. In addition, quiescent studies of accretion-heated NS crusts in LMXBs provide us with the opportunity to probe the properties of dense matter physics. We have examined the crust-cooling source EXO 0748–676 in quiescence. Early in quiescence, this source has behaved like a typical crust-cooling source. However, recently obtained observations indicate an unexpected temperature rise (see Section 1.1). This rise in temperature may be a result of increased low-level accretion in quiescence, although studies of the X-ray spectra indicate that this is likely not the case (see Parikh et al. 2020, for more details). Here, we have further investigated the possibility of ongoing accretion in quiescence in EXO 0748–676 by examining the quiescent FUV spectrum and several epochs of (quasi-)simultaneous X-ray and NUV data.

4.1 The quiescent FUV spectrum

Due to the inherently low quiescent FUV flux of EXO 0748–676, all FUV spectroscopic data had to be stacked to increase the signal to noise and hence no phase-resolved study could be performed. We do not detect FUV continuum emission from the source, but there is one prominent emission line detected, C IV ($\simeq$1550 Å), for which we measure a width of $\gtrsim$18.2 Å ($\gtrsim$3523 km s^{-1}).

The FUV spectrum of this source obtained during the outburst also shows a prominent C IV line (alongside other emission lines), for which we measure a width of $\simeq$19.5 Å. Tomograms made using the outburst data, presented in Pearson et al. (2006), show that the C IV emission may arise from the accretion disc, the accretion impact stream, and the irradiated donor star. Our obtained lower limit on the width of this line in quiescence is close to the value measured during outburst. This could suggest that the line is produced at a similar location. Studies of other LMXBs suggest their quiescent UV emission may arise from the heated inner edge of the accretion disc, the accretion impact stream, and the irradiated donor star (e.g. Froning et al. 2011; Hynes & Robinson 2012; Bernardini et al. 2013; Cackett et al. 2013a). In the following, we investigate what the most likely origin of the quiescent UV emission is for EXO 0748–676.

4.2 No disc/accretion stream in quiescence?

Outburst studies of EXO 0748–676 in the X-ray indicated the presence of 'dipping' features likely due to the presence of an ionized absorber (e.g. Sidoli, Parmar & Oosterbroek 2005). Psaradaki et al. (2018) examined the high-resolution outburst spectra during the eclipses using the reflection grating spectrometer (RGS) on board *XMM–Newton*. Their study found emission lines that may be due to clumps produced by the presence of the accretion stream as it impacts the disc. To investigate whether the C IV line we detect from the source in quiescence may arise from such clumps, we extrapolated their outburst model to the FUV. We have further extrapolated this to quiescence by using the RGS data obtained during early quiescence (see Díaz Trigo et al. 2011, for details). However, no significant emission lines were present in these data and, therefore, the study carried out for the outburst spectrum could not be extended to quiescence. Furthermore, no dipping features have been observed in the X-ray during quiescence, which instead exhibited eclipses with sharp ingresses and egresses (Díaz Trigo et al. 2011; Degenaar et al. 2014). This raises the question whether the obscuring structure, i.e. the disc and/or accretion stream impact point, is present in quiescence.

Optical spectroscopy studies of EXO 0748–676, carried out $\simeq$1 yr into quiescence (Ratti et al. 2012), showed no indications of the presence of an accretion disc (as discerned from the optical line emission). It is worth noting though, that this study was carried out early in quiescence, while our *HST* observations were obtained $\simeq$3.5 yr later and the disc may have built up over time. Such a build-up of the accretion disc may have been observed for another edge-on crust-cooling source, MXB 1659–29. For that source, this scenario was proposed based on a possible increase in the absorption column density as inferred from X-ray spectral fitting (see Cackett et al. 2013b, for details).[10] However, as argued above it is not obvious that this was the case for EXO 0748–676, so we continue to explore other possibilities for the origin of is UV emission.

4.3 Irradiation of the companion star

Although no evidence of an accretion disc was found by Ratti et al. (2012), they observed variations at different orbital phases indicating that the irradiated face of the companion star was emitting in the optical. This raises the possibility that the quiescent UV radiation may also arise due to the irradiation of the companion by the central X-ray source. However, the observed C IV emission line is much broader than the observed optical lines. We measure a lower limit of $\gtrsim$3523 km s^{-1}, whereas the reported widths of the optical spectral lines are $\simeq$300–400 km s^{-1} (see table 1 of Ratti et al. 2012).[11]

Based on their optical study in quiescence, Ratti et al. (2012) suggest that EXO 0748–676 may be a black widow system, in which the pulsar wind interacts with the companion star, slowly obliterating it.[12] This scenario would require the NS in EXO 0748–676 to turn on as a radio pulsar in quiescence. It may then be similar to the handful of known transitional millisecond radio pulsars (tMSRPs) that appear to switch between radio pulsar states and low-luminosity LMXB-like states in which an accretion disc is detected in the system in the optical band.

The optical lines in the spectrum of PSR J1023+0038, one of the tMSRPs, arise from irradiation of the companion star and are narrow (McConnell et al. 2015), like the optical lines of EXO 0748–676 in quiescence (Ratti et al. 2012). The difference in line width makes it unlikely that the C IV emission line observed for EXO 0748–676 arises due to irradiation of the companion star, but the radio pulsar scenario does pose another possibility for its origin.

4.4 Pulsar wind or optically thin accretion disc

Interestingly, the UV lines of PSR J1023+0038 are also very broad ($\simeq$2000–3000 km s^{-1}). Since the accretion disc in this system is truncated very far away from the NS, it was proposed that these lines are produced by the pulsar wind ionizing material from the companion star (i.e. the lines would then be broadened by the velocity of the wind; Hernández Santisteban 2016). Possibly, a similar physical scenario can explain the broadness of the C IV emission line in EXO 0748–676.

Inspecting the red wing of the airglow emission line around $\simeq$1220 Å in the quiescent UV spectrum of EXO 0748–676 suggests that there may be an excess corresponding to the N V emission line that was seen in outburst (Pearson et al. 2006). We cannot confidently constrain its presence, but if this line is there, this could lend support for the pulsar wind scenario. This mechanism has also been invoked to explain the UV excess in two systems hosting tMSRPs (Rivera Sandoval et al. 2018). Nevertheless, this has only been shown for a small sample of sources and similar studies cannot be carried out for EXO 0748–676 as its continuum emission is not detected.

Another possibility, which does not require invoking EXO 0748–676 turns on as a radio pulsar in quiescence, is that material from the companion star is ionized by a geometrically thick, optically thin quiescent accretion flow. If such a flow is present in this system, we might expect material to accrete on to the NS (e.g. Chakrabarty et al.

---

[10]This change was observed $\simeq$11 yr into quiescence and $\simeq$3 yr before MXB 1659–29 was seen to enter a new outburst (Negoro et al. 2015).

[11]We note that the C IV line is actually a doublet, separated by $\simeq$500 km s^{-1}, so it is possible that in our low signal to noise data two lines are merged into one. Nevertheless, the lines would still need to be significantly broader than the lines in the optical quiescent spectrum presented in Ratti et al. (2012).

[12]We note that the constraints on the mass of the donor star yield >0.11 M$_\odot$ for a 'canonical' NS mass of 1.4 M$_\odot$ (see Bassa et al. 2009, and references therein), which means that should EXO 0748–676 be an active pulsar, it would be classed as a redback, like the tMSRPs, rather than a black widow.

2014; D'Angelo et al. 2015). However, there are no signs of ongoing accretion in EXO 0748–676.

4.5 The (lack of) X-ray/UV correlation

In addition to FUV spectra, we have also examined several epochs of quasi-simultaneous X-ray and NUV data in quiescence. If the UV emission arises somewhere in a quiescent accretion flow that reaches the NS, a correlation between the UV and X-ray emission would be expected. Taking into account the uncertainty of the UV spectral shape, we find no evidence for significant changes in the UV emission during quiescence, although the uncertainties are so large that changes of similar magnitude as seen in the X-rays can be hidden within the errors.

Despite that we cannot firmly determine if the X-ray and UV emission change in tandem, the X-ray/UV luminosity ratio gives additional information. We determined the ratio of quiescent X-ray to NUV emission to be $L_X/L_{UV} \gtrsim 100$. Since the UV luminosity of EXO 0748–676 is of similar magnitude as that of other LMXBs, this high ratio would suggest that it is considerably more X-ray bright than other systems (see Fig. 3). In particular, the two NS LMXBs in the sample of Hynes & Robinson (2012), Cen X-4 and Aql X-1, exhibit $L_X/L_{UV} \simeq 10$. In Cen X-4, there is compelling evidence that the intrinsic NUV emission comes from the accretion flow (e.g. Bernardini et al. 2013; Cackett et al. 2013a), and that matter accretes on to the surface of the NS even at these low luminosities (e.g. Chakrabarty et al. 2014; D'Angelo et al. 2015). The same might be true for Aql X-1, which exhibits X-ray variability of several magnitudes in quiescence (e.g. Rutledge et al. 2001; Campana & Stella 2003; Cackett et al. 2011; Coti Zelati et al. 2014). The fact that EXO 0748–676 has a similar UV luminosity as these systems but is much brighter in the X-rays, would then suggest that its X-ray emission is not (predominantly) powered by low-level accretion.

In conclusion, our study of (quasi-)simultaneous UV and X-ray observations of EXO 0748–676 in quiescence hints that the observed broad UV emission line arises from ionization of material from the companion star, possibly by a pulsar wind. Similar to previous optical and X-ray studies, our combined UV/X-ray analysis does not reveal evidence for the presence of a quiescent accretion stream, nor that the high quiescent X-ray emission of EXO 0748–676 arises from ongoing low-level accretion. Our results thus seem to be in favour of explaining the bulk of the quiescent X-ray emission of EXO 0748–676 as cooling of the NS crust. This implies that such studies can be used to infer the properties of the crust and core of this NS (e.g. Degenaar et al. 2011a; Parikh et al. 2020).

DATA AVAILABILITY

The data underlying this article are available in Zenodo, at https://doi.org/10.5281/zenodo.3908291. The data sets were derived from sources in the public domain: https://archive.stsci.edu/hst/sear ch.php, http://nxsa.esac.esa.int/nxsa-web/#home and https://heasar c.gsfc.nasa.gov/cgi-bin/W3Browse/swift.pl.

REFERENCES

Astropy-Specutils Development Team, 2019, Astrophysics Source Code Library, record ascl:1902.012
Bassa C. G., Jonker P. G., Steeghs D., Torres M. A. P., 2009, MNRAS, 399, 2055
Bernardini F., Cackett E., Brown E., D'Angelo C., Degenaar N., Miller J., Reynolds M., Wijnands R., 2013, MNRAS, 436, 2465
Brown E. F., Cumming A., 2009, ApJ, 698, 1020
Brown E. F., Bildsten L., Rutledge R. E., 1998, ApJ, 504, L95
Burrows D. et al., 2005, Space Sci. Rev., 120, 165
Cackett E., Fridriksson J., Homan J., Miller J., Wijnands R., 2011, MNRAS, 414, 3006
Cackett E., Brown E., Degenaar N., Miller J., Reynolds M., Wijnands R., 2013a, MNRAS, 433, 1362
Cackett E., Brown E., Cumming A., Degenaar N., Fridriksson J., Homan J., Miller J., Wijnands R., 2013b, ApJ, 774, 131
Campana S., Stella L., 2003, ApJ, 597, 474
Cardelli J., Clayton G., Mathis J., 1989, ApJ, 345, 245
Carnall A. C., 2017, preprint (arXiv:1705.05165)
Chakrabarty D. et al., 2014, ApJ, 797, 92
Cheng Z., Mendez M., Diaz-Trigo M., Costantini E., 2017, MNRAS, 471, 2605
Coti Zelati F., Campana S., D'Avanzo P., Melandri A., 2014, MNRAS, 438, 2634
Cumming A., Brown E. F., Fattoyev F. J., Horowitz C. J., Page D., Reddy S., 2017, Phys. Rev. C, 95, 025806
D'Angelo C. R., Fridriksson J. K., Messenger C., Patruno A., 2015, MNRAS, 449, 2803
Degenaar N., Wijnands R., 2012, MNRAS, 422, 581
Degenaar N. et al., 2009, MNRAS, 396, L26
Degenaar N. et al., 2011a, MNRAS, 412, 1409
Degenaar N., Brown E. F., Wijnands R., 2011b, MNRAS, 418, L152
Degenaar N. et al., 2014, ApJ, 791, 47
Deufel B., Dullemond C. P., Spruit H. C., 2001, A&A, 377, 955
Díaz Trigo M., Boirin L., Costantini E., Méndez M., Parmar A., 2011, A&A, 528, 150
Done C., Gierliński M., Kubota A., 2007, A&AR, 15, 1
Dubus G., Hameury J.-M., Lasota J.-P., 2001, A&A, 373, 251
Ely J. et al., 2015, IAU General Assembly#29. p. 2255542
Fridriksson J. K., Homan J., Wijnands R., Cackett E. M., Altamirano D., Degenaar N., Brown E. F. et al., 2011, ApJ, 736, 162
Froning C. et al., 2011, ApJ, 743, 26
Froning C. S., Maccarone T. J., France K., Winter L., Robinson E. L., Hynes R. I., Lewis F., 2014, ApJ, 780, 48
Galloway D., Özel F., Psaltis D., 2008, MNRAS, 387, 268
Gehrels N. et al., 2004, ApJ, 611, 1005
Gilfanov M., 2010, in Belloni T., ed. The Jet Paradigm. Lecture Notes in Physics, Vol. 794, X-Ray Emission from Black-Hole Binaries, Springer Berlin, Heidelberg, p. 17
Green J. et al., 2012, ApJ, 744, 60
Haensel P., Zdunik J., 1990, A&A, 227, 431
Haensel P., Zdunik J., 2008, A&A, 480, 459
Hameury J. M., 2020, AdSpR, 66, 1004
Heinke C. O., Rybicki G. B., Narayan R., Grindlay J. E., 2006, ApJ, 644, 1090
Hernández Santisteban J. V., 2016, PhD thesis, https://eprints.soton.ac.uk/40 4707/
Holland S. T. et al., 2012, Cosmic Origins Spectrograph Instrument Handbook for Cycle 21 v. 5.0
Hynes R. I., Haswell C. A., 1999, MNRAS, 303, 101
Hynes R., Jones E., 2008, Astron. Telegram, 1816
Hynes R., Robinson E., 2012, ApJ, 749, 3
Hynes R. I., Robinson E. L., Bitner M., 2005, ApJ, 630, 405

Hynes R. I., Horne K., O'Brien K., Haswell C. A., Robinson E. L., King A. R., Charles P. A., Pearson K. J., 2006, ApJ, 648, 1156

Joseph C. L., et al., 1995, in Johnson B. C., Fenyves E. J., eds, Proceedings of SPIE, Vol. 2551 , Performance Results of the STIS Flight MAMA Detectors, Photoelectronic Detectors, Cameras, and Systems, p. 248

Lasota J.-P., 2001, New Astron. Rev., 45, 449

Mason K. O. et al., 2001, A&A, 365, L36

McConnell O., Callanan P. J., Kennedy M., Hurley D., Garnavich P., Menzies J., 2015, MNRAS, 451, 3468

Narayan R., Yi I., 1994, ApJ, 428, L13

Negoro H., Furuya K., Ueno S., Tomida H., Nakahira S., Kimura M., Ishikawa M. et al., 2015, Astron. Telegram, 7943

Ootes L. S., Wijnands R., Page D., Degenaar N., 2018, MNRAS, 477, 2900

Page D., Reddy S., 2013, Phys. Rev. Lett., 111, 241102

Parikh A. S. et al., 2017, MNRAS, 466, 4074

Parikh A. S., Wijnands R., Homan J., Degenaar N., Wolvers B., Ootes L. S., Page D., 2020, A&A, 638, L2

Parmar A., White N., Giommi P., Haberl F., Pedersen H., Mayor M., 1985, IAU Circ., 4039

Parmar A., White N., Giommi P., Gottwald M., 1986, ApJ, 308, 199

Pearson K. J. et al., 2006, ApJ, 648, 1169

Psaradaki I., Costantini E., Mehdipour M., Díaz Trigo M., 2018, A&A, 620, A129

Ratti E., Steeghs D., Jonker P., Torres M., Bassa C., Verbunt F., 2012, MNRAS, 420, 75

Rivera Sandoval L. E. et al., 2018, MNRAS, 476, 1086

Roming P. W. A. et al., 2005, Space Sci. Rev., 120, 95

Rutledge R., Bildsten L., Brown E., Pavlov G., Zavlin V., 2001, ApJ, 559, 1054

Shakura N. I., Sunyaev R. A., 1973, A&A, 500, 33

Shternin P. S., Yakovlev D. G., Haensel P., Potekhin A. Y., 2007, MNRAS, 382, L43

Sidoli L., Parmar A. N., Oosterbroek T., 2005, A&A, 429, 291

Steiner A. W., 2012, Phys. Rev. C, 85, 055804

Strüder L. et al., 2001, A&A, 365, L18

Tody D., 1986, Proceedings of SPIE, Vol. 0627, The IRAF Data Reduction and Analysis System, Instrumentation in Astronomy VI, p. 733

Torres M., Jonker P., Steeghs D., Seth A., 2008, Astron. Telegram, 1817

Turlione A., Aguilera D. N., Pons J. A., 2015, A&A, 577, A5

Turner M. J. et al., 2001, A&A, 365, L27

Wijnands R., Miller J. M., Markwardt C., Lewin W. H., van der Klis M., 2001, ApJ, 560, L159

Wijnands R., Degenaar N., Padilla M. A., Altamirano D., Cavecchi Y., Linares M., Bahramian A., Heinke C., 2015, MNRAS, 454, 1371

Wijnands R., Degenaar N., Page D., 2017, J. Astrophys. Astron., 38, 49

Wolff M., Becker P., Ray P., Wood K., 2005, ApJ, 632, 1099

Wolff M., Ray P., Wood K., 2008a, Astron. Telegram, 1736

Wolff M., Ray P., Wood K., Wijnands R., 2008b, Astron. Telegram, 1812

Wolff M., Ray P., Wood K., Hertz P., 2009, ApJS, 183, 156

Yan Z., Yu W., 2015, ApJ, 805, 87
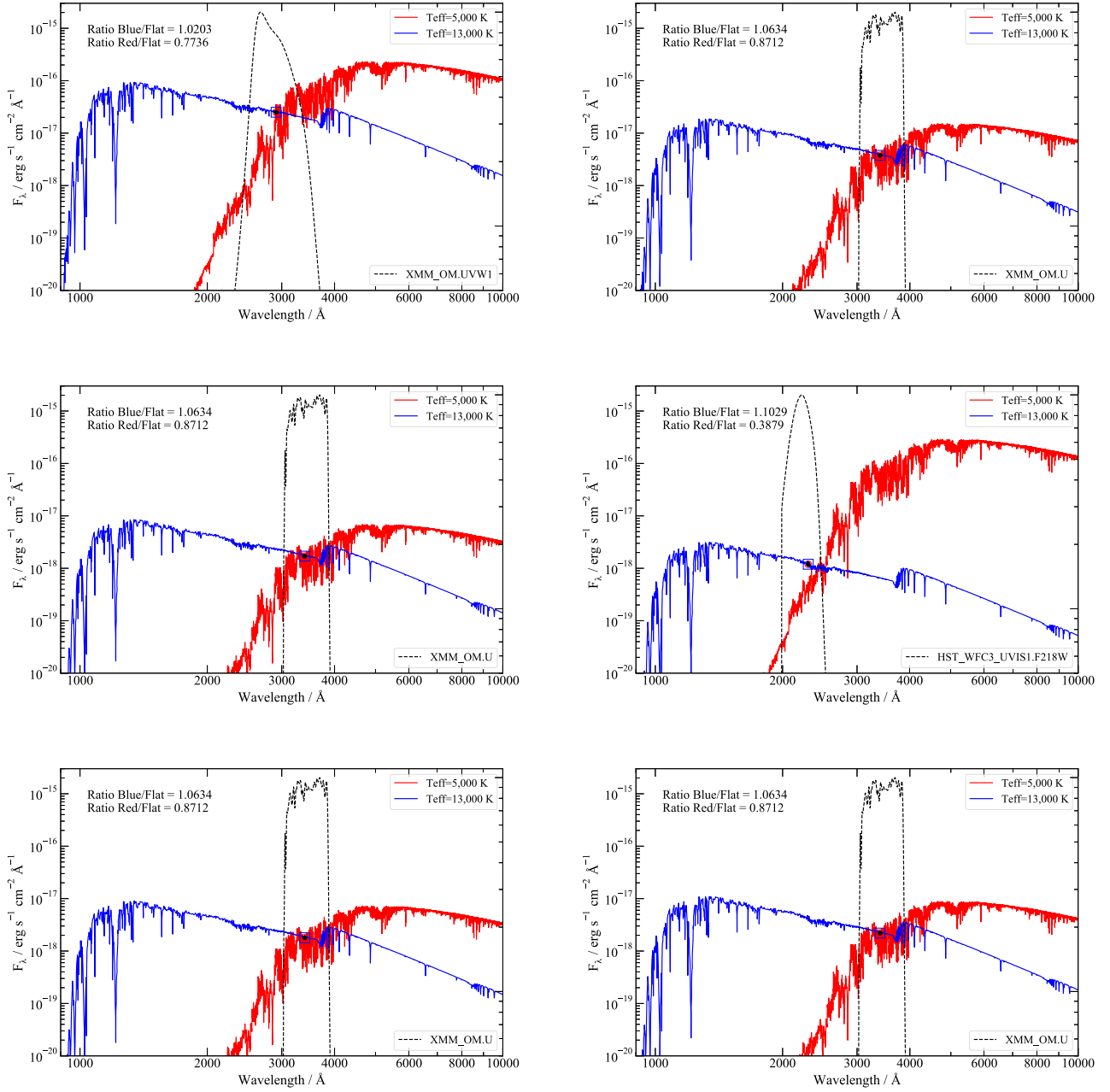
APPENDIX A: UV SPECTRAL SHAPE CORRECTIONS

Figure A1. Estimates of the effect of the unknown UV spectral shape on the inferred UV luminosity. For each observation, we show the measured UV flux (upper limit) as the black data point, while the blue and red curves represent blackbody spectra with temperatures of 13 000 and 5000 K, respectively. The black dashed curves show the different filter transmissions. Printed in the top left are the ratios of the integrated fluxes for these models compared to a flat distribution over the filter passband. These plots show that the unknown spectral shape has a relatively minor impact on the calculated *U*-band luminosity (of order 10 per cent), but has an increasingly large impact for bluer filters.

This paper has been typeset from a TEX/LATEX file prepared by the author.